SADEGH VARMAZIAR[1], HOSSEIN MOSTAAN[1*], MAHDI RAFIEI[2], MAHDI YEGANEH[3]

WELDING AND CORROSION BEHAVIOR OF AISI H13 WELDS: THE EFFECT OF FILLER METAL ON THE MICROSTRUCTURAL EVOLUTIONS

Welding of AISI H13 tool steel which is mainly used in mold making is difficult due to the some alloying elements and it high hardenability. The effect filler metal composition on the microstructural changes, phase evolutions, and hardness during gas tungsten arc welding of AISI H13 hot work tool steel was investigated. Corrosion resistance of each weld was studied. For this purpose, four filler metals i.e. ER 312, ER NiCrMo-3, ER 80S, and 18Ni maraging steel were supplied. Potentiodynamic polarization test and electrochemical impedance spectroscopy (EIS) were used to study the corrosion behavior of weldments. It was found the ER 80S weld showed the highest hardness owing to fully martensitic microstructure. The hardness in ER 312 and ER NiCrMo3 weld metals was noticeably lower than that of the other weld metals in which the microstructures mainly consisted of austenite phase. The results showed that the corrosion rate of ER 312 weld metal was lower than that other weld metals which is due to the high chromium content in this weld metal. The corrosion rate of ER NiCrMo-3 was lower than that of 18Ni maraging weld. The obtained results from EIS tests confirm the findings of potentiodynamic polarization tests.

Keywords: AISI H13 tool steel, Gas tungsten arc welding, Filler metal, Corrosion, Microstructure

1. Introduction

One of the main important factors in mold design and manufacturing is selection of proper material. The selected material for mold making should satisfy both essential parameters i.e. design criteria (toughness, fatigue resistance, wear and corrosion resistances) and fabrication criteria (hardness, machinability, polishability and dimensional stability). AISI H13 is a hot work tool steel containing chromium, molybdenum and vanadium which is extensively used in mold making industries. This tool steel presents some advantageous such as good abrasive wear, resistance at room and elevated temperatures, high toughness, excellent machinability, high strength at high temperatures, resistance to thermal fatigue, and high hardenability [1,2]. These steels are frequently used in making high pressure casting molds, extrusion molds, plastic injection molds, and hot forging molds [3]. These molds which are applied in the fabrication of metallic plates and forging of various products are damaged during service conditions due to the impacts, cyclic loads, corrosion and thermal stresses. This condition leads to the plastic deformations, dimensional instability, formation of surface cracks, and undesired changes in mold geometry. The produced pieces from the damaged mold are not acceptable and are rejected from quality control point of view [4]. Hence, the productivity is very low in this situation. Mold making is an expensive process and cost of machining and polishing of molds is more than 60% of final cost [5,6]. Repair welding is a cost effective method to reduce the costs of mold making and to prolong the service life of the molds [7-9]. Many researchers have reported successfully repairing of damaged molds [10-12].

For this purpose, gas tungsten arc welding (GTAW) which is one of the most prevalent and popular methods for repair welding, is extensively used in the industries. The process which is used for repairing should has some features such as low cost, easy to use, and portability [13]. This process is an interesting method among welding processes owing to its high arc stability, good control in dilution and deposition rate, and very low spatters [14-16]. Moreover, this process is cost effective and the produced weld by this process can be effectively controlled by selecting proper filler metal depending on the service condition of mold. Overall, GTAW equipment is portable and the operator can easily handle the torch when preparing complex parts of a mold [7,17,18].

1   FACULTY OF ENGINEERING, DEPARTMENT OF MATERIALS AND METALLURGICAL ENGINEERING, ARAK UNIVERSITY, ARAK 38156-8-8349, IRAN
2   ADVANCED MATERIALS RESEARCH CENTER, DEPARTMENT OF MATERIALS ENGINEERING, NAJAFABAD BRANCH, ISLAMIC AZAD UNIVERSITY, NAJAFABAD, IRAN
3   DEPARTMENT OF MATERIALS SCIENCE AND ENGINEERING, FACULTY OF ENGINEERING, SHAHID CHAMRAN UNIVERSITY OF AHVAZ, AHVAZ, IRAN

*   Corresponding author: h-mostaan@araku.ac.ir

Besides, thermal and mechanical stresses which are applied to the mold during service conditions, the mold may be led to the corrosion induced damages of mold. So, corrosion mechanism is another factor which could reduce the life of mold. Corrosion process in molds can be accelerated at elevated temperatures caused by molten plastic and molten metal or hot forged pieces. Corrosion is often associated with rapier welded molds, since the microstructure, properties, composition of the weld metal, and HAZ may be quite different than those of the base metal. Corrosion takes a number of forms and may result in general (uniform), localized, or microstructure specific attack. Often, the corrosion rate associated with welds is much higher than the base metal. The reason for this is usually a combination of the effect of microstructure and residual stresses. Highly stressed regions surrounding welds may result in accelerated corrosion relative to the base metal [19]. So, it is essential to prevent the formation of very hard and brittle phases in the weld areas. Besides, proper chemical composition in this area should be considered to prevent the crack formation or initiation and reduce the level of residual stresses. On the other hand, in the inhomogeneous or heterogeneous welding (when the composition of filler metal is different from the base metal), the microstructure and chemical composition of the weld area is completely different from heat affected zone (HAZ) and base metal due to the heating and cooling cycles [20]. Besides, the compositional changes in the weld area, segregation of the alloying elements due to the solidification, and local galvanic attack which may be occurred can lead to more sever corrosion [20, 21]. Selecting an appropriate filler metal for repair welding based on literature can amend service lifetime of damaged molds and even increase the corrosion resistance of weld area higher than that of base metal.

To the author's knowledge, no article has been published concerning the corrosion behavior of AISI H13 weldment. Also, no works are devoted to the effect of filler metal composition on the microstructural evolutions during welding process of AISI H13 hot work tool steel. In this research work, plates of AISI H13 hot work tool steel were welded with GTAW process using four filler metals including ER 80S, ER 312, ER NiCrMo3, and 18Ni 300 maraging steel. After that, microstructural and phase evolutions during welding and also microhardness measurements were conducted. In this research, 18Ni 300 maraging steel was used for the first time. The main aim of this article is throwing a fresh look on the quality of repair welded molds by relating the microstructural state and phase evolutions with the corrosion resistance of the welded areas.

The authors believe that the obtained results would help with exploiting full advantages of the AISI H13 tool steels. The authors believe that the obtained results would help with exploiting full advantages of the AISI H13 tool steels.

2.Materials and experimental procedures

The studied base metal in this research was AISI H13 hot work tool steel. Specimens with dimensions of 150×40×5 mm^3 were prepared using electro discharge machining. The chemical composition of the base metal is provided in Table 1.

TABLE 1

Chemical composition of the applied AISI H13 as base material

Element	C	Si	Mn	Cr	Mo	V
(wt. %?)	0.39	1.0	0.4	5.3	1.3	0.9

After that, the specimens were checked visually and the edges of specimens were ground by sand paper and then cleaned by acetone to remove any contaminations in order to avoid the formation of some defects such as lack of fusion or hydrogen induced cracks. Four different filler metals i.e. ER 80S, ER 312, ER NiCrMo3, and 18Ni 300 maraging steel with diameter of 2.4 mm were used for welding of AISI H13 test plates. The chemical compositions of the used filler metals are shown in Table 2.

The welding of test plates was carried out using GTAW with DCEN polarity. Preheat and interpass temperatures were selected 25 and 100°C, respectively. Also, the welding process was done in 1G position and argon gas with purity level of 99.999% was used to prevent the effects of moisture and contaminations that otherwise may cause porosity formation, cracking, and also suppressing the plasma formation during welding. Low angle value was selected for weld groove to reduce the evaporation of some elements from the base material. So, single 45°'V' groove butt joint configuration was prepared to obtain GTAW joints. The schematic view of the welding process is shown Fig. 1.

Argon shielding gas was provided at a flow rate of 8 l/min and the welding process was performed by a travel speed of about 2 mm/s in two passes. Before beginning the second pass, the lower pass was cleaned carefully to remove any probable oxide layers. The current and voltage for the welding process were selected 150 A and 20 V, respectively. These parameters were kept unchanged when using different filler metals. Accord-

TABLE 2

Chemical compositions of filler metals used in this study

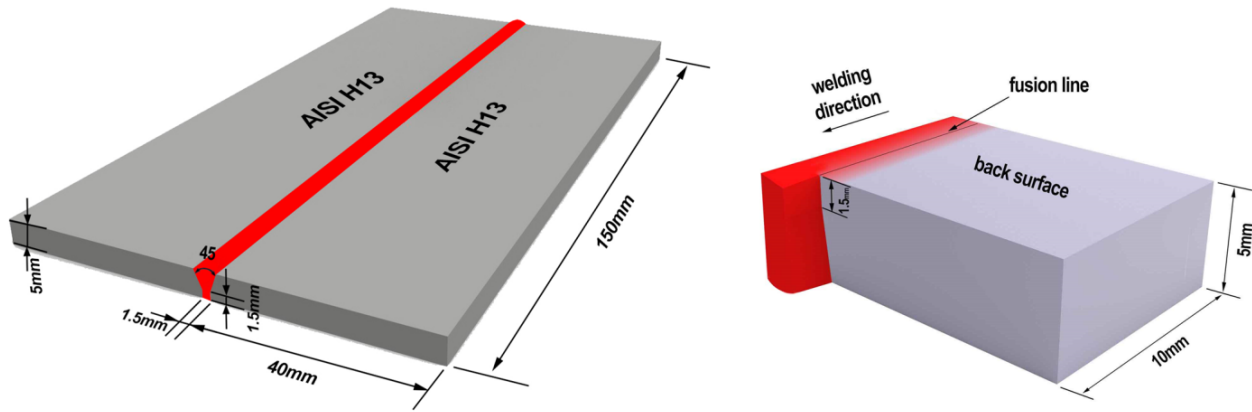| Element	Fe	C	Ni	Cr	Mo	Si	Mn	Cu	Co	Nb	Ti
ER 80S	Bal.	0.07	0.45	5.25	0.5	0.04	0.6	0.2	—	—	—
ER 312	Bal.	0.11	9.25	29	0.15	0.4	1.6	—	—	—	—
ER NiCrMo3	2	0.03	Bal.	21.7	9.3	0.4	0.2	—	—	3.3	—
18Ni 300	Bal.	0.014	—	—	4.81	0.02	0.05	—	8.82	—	0.66

Fig. 1. Schematic representation of the joint design and dimensions of the base metal

ing to the above mentioned parameters and based on Eq. 1, the heat input can be calculated as follows:

$$Heat\ Input = \eta \frac{V \times I}{1000 \times S} = 0.7 \frac{20 \times 150}{1000 \times 2} = 1.05\ kj/mm \quad (1)$$

The samples for microstructural studies and assessment of the phase evolutions were cut from welded joint at 50 mm behind the trailing edge of the crater to eliminate the end effects. The sample preparation and polishing were performed according to the ASTM E 3-11standard. The etchant solution to reveal the microstructures of ER 80S and 18Ni 300 maraging welds was 100 ml distilled water containing 5 g of $FeCl_3$. Also, mixed acid solution (equal parts of HCl, HNO_3 and acetic acid) was used as etchant for ER NiCrMo3 and ER 312 welds. The hardness of the weld joints was determined by microhardness measurements using a Vickers diamond indenter at a load of 100 g and dwell time of 15 s. For each zone, microhardness measurements were taken from three points at an interval of four times the indenter size to avoid the effects of localized strain hardening in the vicinity of the indentation. Finally, the averages of three measurements were reported.

For electrochemical measurements, samples from the welded area with dimensions of $4 \times 4 \times 2$ mm^3 were prepared. Prior to the testing, the samples were abraded with progressively finer SiC paper (up to grit of 2000) and then degreased in ethanol. All the electrochemical corrosion studies were conducted using a three-electrode cell in which a Pt plate and an Ag/AgCl were used as a counter and a reference electrode, respectively. Electrochemical tests were performed on the ER 80S, ER 312, ER NiCrMo3 and 18Ni 300 maraging plates with an exposed area of 0.1 cm^2 as the working electrode. The electrochemical analyses were conducted using an AUTOLAB PGSTAT 302N potentiostat controlled by NOVA software. The electrochemical measurements including electrochemical impedance spectroscopy (EIS) and potentiodynamic polarization were carried out to analyze the corrosion inhibition efficiency of LMT in 3.5 wt. % NaCl. The EIS measurements were carried out at OCP in a frequency range of 100 kHz to 10 mHz with an applied AC signal of 10 mV. The equivalent circuit simulation program (ZView 3.1) was used for data analysis, the equivalent circuit synthesis and

the experimental data fitting. Polarization plots were recorded by changing the electrode potential from –400 to +400 mV vs. Ag/AgCl with a scan rate of 1 mVs^{-1}. Tafel extrapolation method was used to obtain polarization parameters including corrosion current density (i_{corr}), corrosion potential (E_{corr}), and cathodic and anodic slopes (β_c and β_a).

3. Results and discussion

The optical micrograph from the microstructure of AISI H13 base metal is shown in Fig. 2. As can be seen, the base metal is in the as-quenched condition and some retained austenite (white regions) and also some carbide phases such as $M_{23}C_6$ and M_7C_3 are dispersed in the matrix [22]. Discussing about microstructural changes and phase evolution of the welded sample with different filler metals is included in the following sections. It has been reported by some researchers that the main factor in controlling of phase evolutions during fusion welding processes is heat input [23-25]. As mentioned earlier, the thickness of all samples are equal and similar current, voltage, and travel speed were considered for welding by four different filler metals. So, the heat input for each sample remains unchanged and conse-
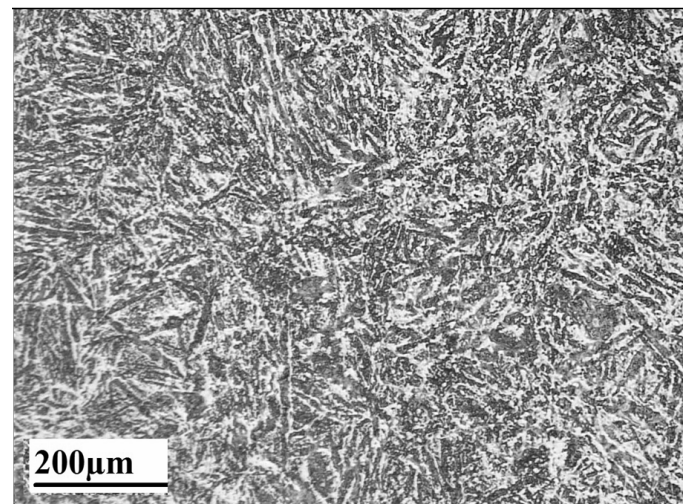

Fig. 2. Optical micrograph of AISI H13 base metal

TABLE 3

The Chemical composition of each weld metal

Element	Fe	C	Ni	Cr	Mo	Si	Mn	Nb	Co
ER 80 S	Bal.	0.61	0.18	5.3	0.74	0.58	0.54	—	—
ER 312	Bal.	0.197	6.47	21.9	0.495	0.58	1.24	—	—
ER NiCrMo-3	1.4	0.141	Bal.	16.79	6.9	0.58	0.26	2.31	—
18 Ni 300	Bal.	0.13	12.6	1.6	3.75	0.31	0.155	—	6.16

quently it can be said that any difference in phase evolution in various welds is only influenced by changes in the chemical composition of filler metals. But, it should be mentioned that the composition of the weld metal is affected by composition of the base metal, filler metal, and also by the degree of dilution [25].

The microstructural features of ER 80S, ER 312, ER NiCrMo3, and 18 Ni maraging weld joints at the center of fusion zone are discussed in the following.

The chemical composition of each weld metal is shown in Table 3.

The microstructure of the weld joint deposited by ER 80S filler metal is shown in Fig. 3. Regarding non-equilibrium solidification during welding process, the martensite layers is formed in the fusion zone. As can be seen, the martensite layers in this area are parallel which are surrounded by retained austenite (the white region in the micrograph). This microstructure is mainly due to the low percentage of carbon in this area (lower than 0.6 wt. %).

The solidification microstructure of ER NiCrMo3 weld metal center is shown in Fig. 4. As known, this filler metal is

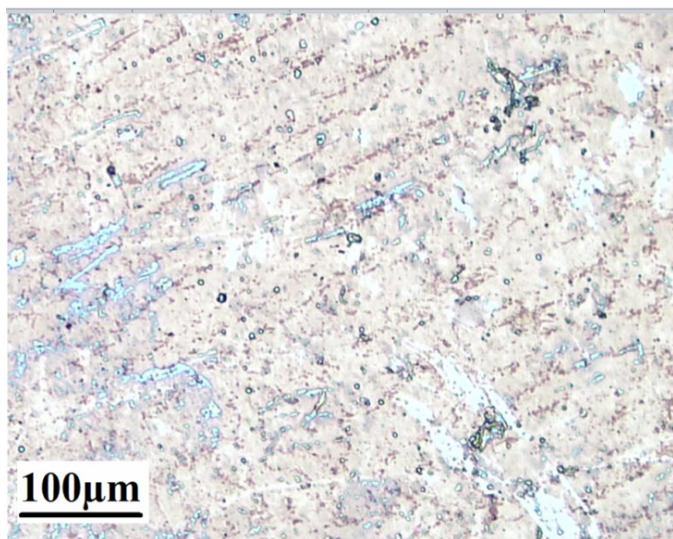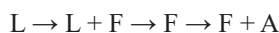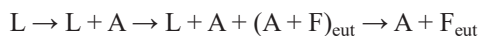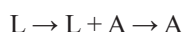Fig. 3. Optical micrograph from the center of ER 80S weld metal

Fig. 4. Optical micrograph from the center of ER NiCrMo3 weld metal

a nickel based filler metal and it is expected that the main phase in the weld metal would be austenite. According to the chemical composition of the base metal and ER NiCrMo3 filler metal and based on the WRC and Schaeffler diagram, any delta ferrite can be formed in the fusion zone and solidification will begin by the formation of austenite phase. Cr and Nb-rich carbides are formed in the weld metal at the end of solidification by decreasing in the solubility of the alloying element due to the cooling process.

Fig. 5 shows the solidification microstructure of ER 312 weld metal. As shown earlier, this filler metal contains ~10 wt. % of nickel and is an austenitic filler metal. So it is anticipated that the austenite phase forms in the weld metal [26]. The micrograph shown in Fig. 5 indicates the presence of austenite phase in the microstructure. It has been shown that there are four solidification and solid state possibilities for austenitic weld metals. These reactions are shown below and are related to Fe-Ni-Cr phase diagram [25].

$$L \rightarrow L + A \rightarrow A$$
$$L \rightarrow L + A \rightarrow L + A + (A + F)_{eut} \rightarrow A + F_{eut}$$
$$L \rightarrow L + F \rightarrow L + F + (F + A)_{eut} \rightarrow F + A$$
$$L \rightarrow L + F \rightarrow F \rightarrow F + A$$

It should be mentioned that the two first solidification modes are associated with the primary austenite solidification. In the case of two last modes, the solidification begins with formation of delta ferrite. After the solidification and by further cooling, the ferrite phase is decomposed to other phase due to the instability [27]. There is ~30 wt. % of chromium in the ER 312 filler metal. Therefore, the weld metal is consisted of a high percentage of chromium which is a ferrite stabilizer alloying element and formation of delta ferrite is expected in the weld metal. The formation of martensite is not probable and, therefore a low hardness value was recorded in this weld metal which indicates martensite phase is not formed in this area. On the other hand, Cr-rich carbides are formed in ER 312 weld metal regarding the high level of chromium and decrease in its solubility during further cooling.

The optical micrograph of 18 Ni maraging weld metal is shown in Fig. 6. This filler metal is also contains a high percentage of nickel and two columnar and cellular dendritic microstructure and also difference between dendrite arm spacing can be seen in the micrograph. The changes in solidified microstructures can be explained by constitutional undercooling. It is well established that the ratio of G (temperature gradient) to R (solidification rate) decreases from fusion line toward center line. This suggests that the solidification mode may change from cellular to columnar across the fusion zone [28]. The dendrite arm spacing is mainly affected by $G \times R$ parameter. This parameter describes the cooling rate of the weld metal and decreases from fusion line toward center line. Thus, the reduction in arm spacing of dendrite from center line toward fusion line is expected. These changes are indicated by Fig. 6 and it should also be noted that the microstructure is mainly consisted of austenite phase since the filler metal contains about 18 percent of nickel as an austenite stabilizer element.

3.2. Microhardness measurement

The microhardness of the weld metals at the center line was investigated and the obtained results are shown in Table 4 and are compared in Fig. 7. The reported values are actually the average of three test results. As shown in Fig. 7, the ER 80S weld metal
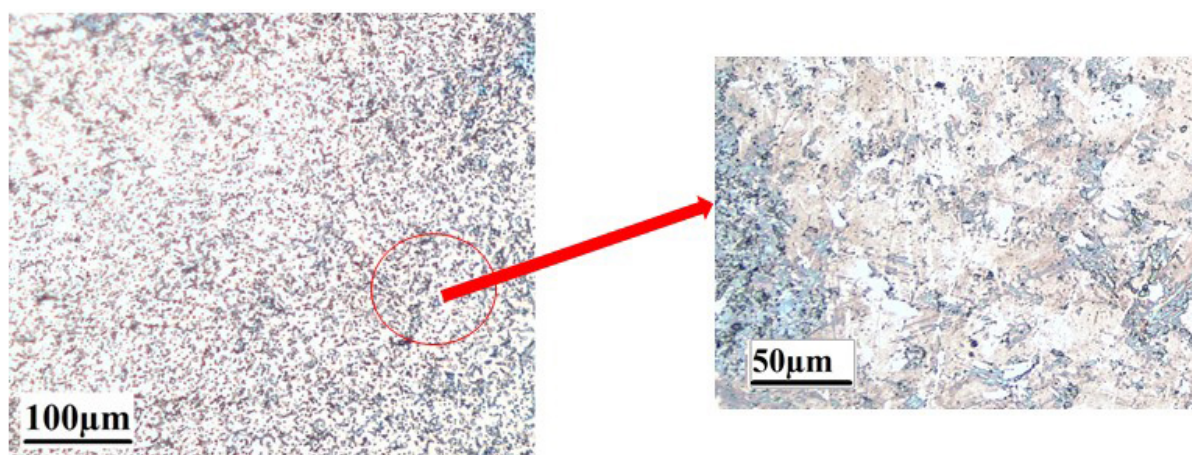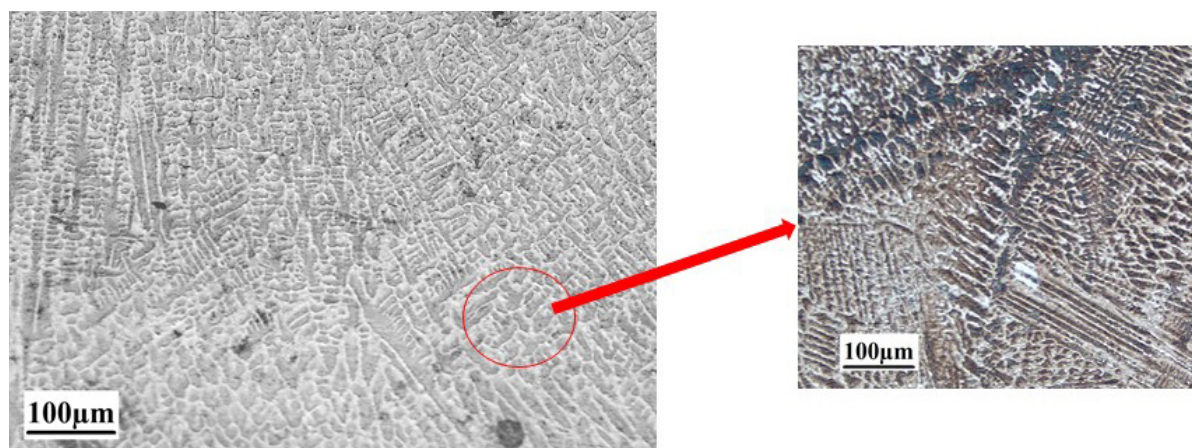

Fig. 5. The microstructure of ER 312 weld metal

Fig. 6. The microstructure of 18 Ni maraging weld metal

TABLE 4

Microhardness measurement of various filler metal welding zone

Filler Metal	1	2	3	Ave.
ER 80S-G	489.13 HV0.1	431.99 HV0.1	448.26 HV0.1	456.46 HV0.1
ER 312	294.22 HV0.1	288.78 HV0.1	291.86 HV0.1	291.62 HV0.1
ER NiCrMo-3	245.85 HV0.1	241.45 HV0.1	243.06 HV0.1	243.45 HV0.1
Maraging	462.42 HV0.1	424.95 HV0.1	424.95 HV0.1	437.44 HV0.1

has the highest hardness of 456.46 Vickers. As mentioned above, the microstructure of this weld metal is mainly consisted of martensite phase. Therefore, it is obvious the ER 80S weld metal should has the maximum hardness. Moreover, in 18Ni maraging weld metal, the hardness is near to the ER 80S weld metal (~440 Vickers). The presence of a fine equiaxed microstructure is the main reason for developing a high hardness in this weld metal. The hardness in ER 312 and ER NiCrMo3 weld metals is noticeably lower than that of the other weld metals. This can be attributed to the fully austenitic microstructure in the weld metal resulting to the lack of hard phases in this area. On the other hand, the hardness of ER NiCrMo3 weld metal is lower than that of ER 312 weld metal. As it known, the solubility limit of chromium in iron (ER 312) is lower than solubility of chromium in nickel (ER NiCrMo3). So, during cooling of ER 312 weld metal, a more fraction of hard carbide precipitates is formed. In addition, the ER 312 weld metal has a dual phase microstructure (delta ferrite + austenite) which indicates a more fraction of grain boundaries in this weld metal. These two factors, i. e. more carbide precipitates and presence a dual phase microstructure in ER 312 weld metal lead to higher hardness in this weld metal.
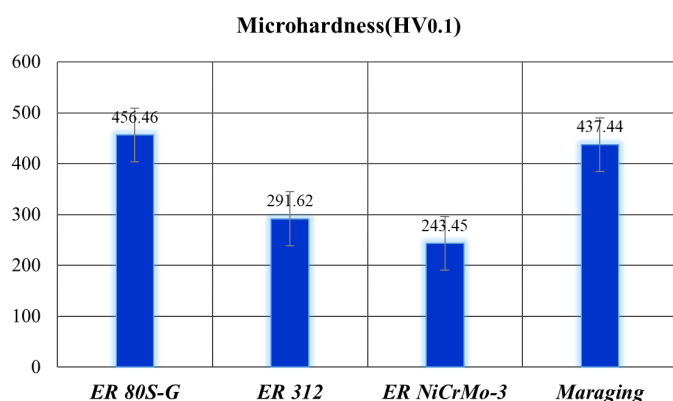
Corrosion current density (I_{corr}), corrosion potential (E_{corr}), cathodic slope (β_c), and anodic slope (β_a) were extrapolated from the polarization curves which are reported in Table 5. In addition, linear polarization resistance (R_p) was calculated using Stern-Geary equation (See Eq. 4) [29]. It should be mentioned that all of these data were obtained by means of EC-Lab software.

$$R_P = \frac{\beta_a \times \beta_c}{2.303 I_{Corr}(\beta_a + \beta_c)} \tag{4}$$

It is well established that the corrosion current density plays an important role in determining the corrosion rate of materials [30]. According to the obtained results from polarization test (Fig. 8 and Table 4), it can be concluded that the ER 312 weld metal has the lowest corrosion current density of 0.651 µA/cm².

TABLE 5

The data and corrosion parameters of samples welded by different weld metals

Filler Metal	I_{corr} (µA/cm²)	E_{corr} (mV)	β_a (mV)	β_c (mV)	R_p (Ω.cm²)
ER 80S-G	1.790	–419.709	60.6	575.8	13.3
ER 312	0.651	–374.338	154.3	300.5	68.00
ER NiCrMo-3	1.339	–421.296	92.4	407.3	24.06
Maraging	2.409	–353.145	98.9	683.1	15.57

ER NiCrMo3 filler metal has also a low corrosion current density but higher than that of ER 312 weld metal. These two filler metals have a large amount of chromium and regarding to the higher percentage of this alloying element in ER 312 filler metal, a lower corrosion current density is expected in comparison to other weld metals. Polarization resistance can be used to evaluate the corrosion rate of the weld metals [31]. As shown in Table 4, the polarization resistance of ER 312 weld metal is minimum comparing to other weld metals which indicates the lowest corrosion rate in the weld metals deposited by ER 312 filler metal. Although the 18 Ni maraging weld metal has a lower corrosion current density than that of ER 80S weld metal, but regarding its larger corrosion potential relative to other weld metals and also owing higher polarization resistance comparing with ER 80S weld metal, showing a better corrosion resistance than that of ER 80S weld metal.

Cathodic branches of all samples present the similar behavior, while the anodic branches show the different situation. It could be explained by the different anodic dissolution rate corresponding the different phases present in the microstructure. Besides, ER312 weld depicts the lowest current in the anodic

Fig. 7. Typical Vickers-microhardness observed in the different weld metal cross sections

3.3. Corrosion behavior

3.3.1. Potentiodynamic polarization corrosion test

The potentiodynamic polarization curves which were obtained from the center of four weld metals are shown in Fig. 8. These corrosion tests were conducted in 3.5 wt. % NaCl solution at room temperature. This test can be effectively used to evaluate the corrosion current and corrosion resistance of each weld metal.

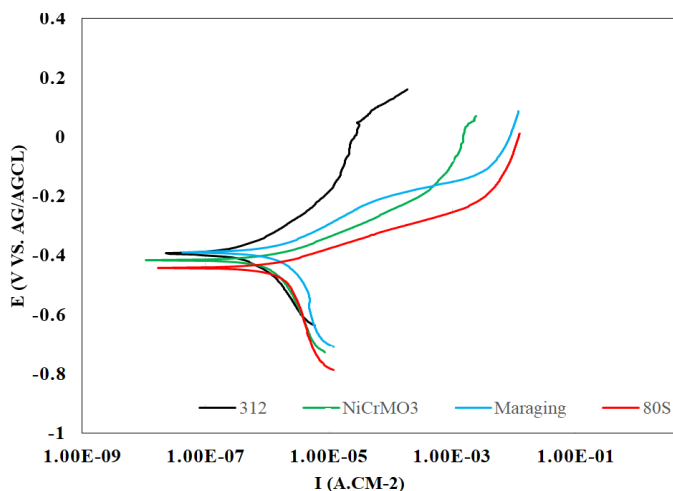region compared to the other one indicating the higher corrosion resistance in the harsh situation.

Fig. 8. The Tafel slope for different weld metals

3.3.2. Electrochemical impedance spectroscopy

The Nyquist plots of each weld metal which are obtained using electrochemical impedance spectroscopy are shown in Fig. 9. As shown in this figure, the plots for all of the weld metals show a circle indicate a capacitive behavior. Equivalent circuits for all of the metals are similar and are shown in Fig. 10. The circuit elements for obtained data include a solution resistance, R_s, and a charge transfer resistance, R_{ct}, and a constant phase element, CPE. R_s is the solution resistance between the reference and the working electrodes, and R_{ct} represents the charge-transfer resistance at the Metal/electrolyte interface. In addition, the R_{ct} value is mirrored in the diameter of the capacitive loop and has a direct proportionality with the corrosion resistance. R_{ct} could be defined as the value corresponding to Z' when $-Z'' = 0$, which is commonly obtained at intermediate frequencies [32]. CPE was used instead of a pure capacitance (C) accounting for non-ideal capacitive response of the interface. The impedance of a CPE is equal to $A^{-1} (i\,\omega)^{-n}$, where A is the constant corresponding to the interfacial capacitance, i is the imaginary number, ω is the angular frequency, and n is an exponential factor in the range between -1 and 1. Depending on the value of n, CPE can illustrate resistance ($n = 0$, $A = R$), capacitance ($n = 1$, $A = C$), inductance ($n = -1$, $A = L$), and Warburg impedance ($n = 0.5$, $A = W$) in the different situations. Pure capacitance behavior is indicated by $n = 1$, while in practice n often ranges from zero to 1 [32].

The data obtained for Nyquist curves are listed in Table 6.

The diameter of extrapolated circle in Nyquist curve shows the charge transfer resistance which is demonstrated by R_{ct} [33]. Consequently, larger circle diameter means a larger R_{ct} and therefore the corrosion rate would be lower [34]. As it is shown in Fig. 9, the diameters of circles decrease from ER 312 to ER 80S weld and consequently it can be said that the ER 312 weld has lowest corrosion rate while ER 80S weld has maximum corro-

TABLE 6

The obtained data from Nyquist curves of different weld metals in the NaCl solution

Filler Metal	R_s ($\Omega.cm^2$)	CPE T ($\mu F.cm^{-2}$)	CPE-P ($\mu F.cm^{-2}$)	R_p ($\Omega.cm^2$)
ER 80S-G	31.83	4.0342×10^{-5}	0.66848	11439
ER 312	37.97	1.4966×10^{-5}	0.73759	49127
ER NiCrMo-3	31.02	1.7574×10^{-5}	0.73311	22362
Maraging	30.81	2.8336×10^{-5}	0.76245	12623

sion rate. On the other hand, the corrosion rate of ER NiCrMo-3 is lower than that of 18Ni maraging weld. Accordingly, the obtained results from EIS tests confirm the findings of potentiodynamic polarization tests.
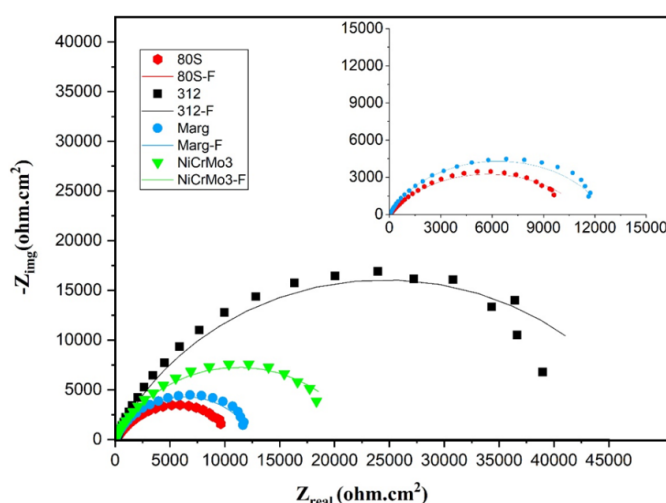

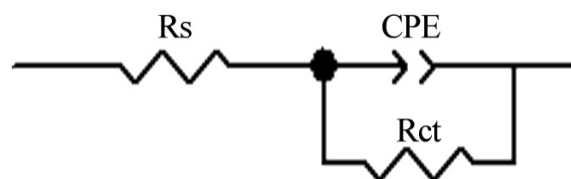Fig. 9. The Nyquist curves for different weld metals in the 3.5 wt. % NaCl

Fig. 10. Electrochemical circuit (Randles cell)

4. Conclusions

Similar butt welding of AISI H13 hot work tool steel plates was studied using GTAW. For this purpose, four different filler metals (ER 312, ER 80S, ER NiCrMo-3 and 18 Ni maraging steel) were used. The welding operation was done successfully. Microstructural observation and phase evolutions were investigated and the effect of filler metal composition on the corrosion rate of weld metals was studied. Based on the obtained data the main findings of this research are as follows:

1. ER 80S filler metal led to a fully martensitic structure in the fusion zone and heat affected zone and hence a high hardness was obtained.

846

2. ER 312 and ER NiCrMo-3 filler metals had the lowest hardness owing to the presence of austenite as major phase in the weld metal.

3. The sample welded by ER 312 filler metal had lowest corrosion rate, whilst ER 80S showed a low corrosion resistance.

4. The presence of chromium in the ER 312 and ER NiCrMo-3 weld metals was the main factor which led to increase in corrosion resistance.

5. 18 Ni maraging weld metal had a lower corrosion current density than that of ER 80S weld metal, but regarding its larger corrosion potential relative to other weld metals and also owing higher polarization resistance comparing with ER 80S weld metal, showed a better corrosion resistance than that of ER 80S weld metal.

REFERENCES

[1] B. Uddeholm, Bohler-Uddeholm H13 tool steel, 2013.

[2] J. Wang, Z. Xu, and X. Lu, J. Mater. Eng. Perform. **29** (3), 1849-1859 (2020).

[3] G.A. Roberts, R. Kennedy, G. Krauss, Tool steels, 1998 ASM international.

[4] S. Jhavar, C.P. Paul, N.K. Jain, Eng. Fail. Anal. **34**, 519-535 (2013).

[5] R.A. Meaquita, C.A. Barbosa, Proceedings of Machining, 2004 Sao Paulo.

[6] R.A. Mesquita, R. Schneider, Exacta. **8** (3), 307-318 (2010).

[7] W.T. Preciado, C.E.N. Bohorquez, Mater. Process. Technol. **179** (1-3), 244-250 (2006).

[8] A. Skumavc, J. Tušek, M. Mulc, D. Klobčar, Metalurgija. **53** (4), 517-520 (2014).

[9] J. Chen, S.-H. Wang, L. Xue, Mater. Sci. **47** (2), 779-792 (2012).

[10] A. Košnik, J. Tušek, L. Kosec, T. Muhič, Metalurgija. **50** (4), 231-234 (2011).

[11] S. Thompson, Handbook of mould: Tool and die repair welding, 1999 Elsevier.

[12] T. Branza, A. Duchosal, G. Fras, F. Deschaux-Beaume, P. Lours, Mater. Process.

[13] P. Peças, E. Henriques, B. Pereira, M. Lino, M. Silva, Build Futur. Innov. (2006).

[14] L.E.E. Jae-Ho, J. Jeong-Hwan, J.O.O. Byeong-Don, Y.I.M. Hong-Sup, M. Young-Hoon, Trans. Nonferrous Met. Soc. China. **19**, 284-287 (2009).

[15] S.U.N. Yahong, S. Hanaki, H. Uchida, H. Sunada, N. Tsujii, Mater. Sci. Technol. **19**, 91-93 (2009).

[16] R.H.G. e Silva, L.E. dos Santos Paes, C. Marques, K.C. Riffel, M.B. Schwedersky, J. Brazilian Soc. Mech. Sci. Eng. **41** (1), 38 (2019).

[17] K. Somlo, G. Sziebig, Ifac-papersonline. **52** (22), 101-107 (2019).

[18] J.-L. Desir, Eng. Fail. Anal. **8** (5), 423-437 (2001).

[19] J.C. Lippold, Welding metallurgy and weldability, 2015 Wiley Online Library.

[20] J.R. Davis, Corrosion of weldments, 2006 ASM international.

[21] R.G. Buchheit Jr, J.P. Moran, G.E. Stoner, Corrosion. **46** (8), 610-617 (1990).

[22] K.A. Chiang, Y.C. Chen, Mater. Lett. **59** (14-15), 1919-1923 (2005).

[23] C.F.G. Baxter, J. Irwin, R. Francis, The Third International Offshore and Polar Engineering Conference, 1993.

[24] M. Liljas, Glas. Scotland, Keynote Pap. V. **2**, 13-16 (1994).

[25] J. Lippol, J.K. Damian, Welding metallurgy and weldability of stainless steels, 2005 John Wiley & Sons, New York.

[26] J.C. Lippold, S.D. Kiser, J.N. DuPont, Welding metallurgy and weldability of nickel-base alloys, 2011 John Wiley & Sons.

[27] R.M. Rasouli I, Metall. Eng. **21** (1), 54-71 (2018).

[28] S. Kou, Welding metallurgy, 2003 John Wiley & Sons, New Jersey.

[29] M. Stern, A.L. Geary, Electrochem. Soc. **104** (1), 56-63 (1957).

[30] Y. Zhang, J. You, J. Lu, C. Cui, Y. Jiang, X. Ren, Surf. Coatings Technol. **204** (24), 3947-3953 (2010).

[31] E.E. Stansbury, R.A. Buchanan, Fundamentals of electrochemical corrosion, 2000 ASM international.

[32] M. Yeganeh, M. Saremi, Prog. Org. Coatings. **79**, 25-30 (2015).

[33] P. Langford, J. Broomfield, Constr. Repair. **1** (2), (1987).

[34] A. Aguilar, A.A. Sagüés, R.G. Powers, Corrosion Rates of Steel in Concrete, 1990 ASTM International.